Journal of Power Sources 244 (2013) 56–62

Contents lists available at SciVerse ScienceDirect

Journal of Power Sources

journal homepage: www.elsevier.com/locate/jpowsour

One step preparation of Mn_3O_4/graphene composites for use as an anode in Li ion batteries

Inho Nam [1], Nam Dong Kim [1], Gil-Pyo Kim, Junsu Park, Jongheop Yi*

World Class University Program of Chemical Convergence for Energy & Environment, School of Chemical and Biological Engineering, Institute of Chemical Processes, Seoul National University, Seoul 151-742, Republic of Korea

HIGHLIGHTS

- An in-situ transformation method was developed for fabricating a Mn_3O_4/GNS composite.
- Two step reactions, Mn^{2+} oxidation and GO reduction, are simultaneously carried out.
- The Mn_3O_4/GNS composite has a high capacity in low cost without toxic byproducts.

GRAPHICAL ABSTRACT

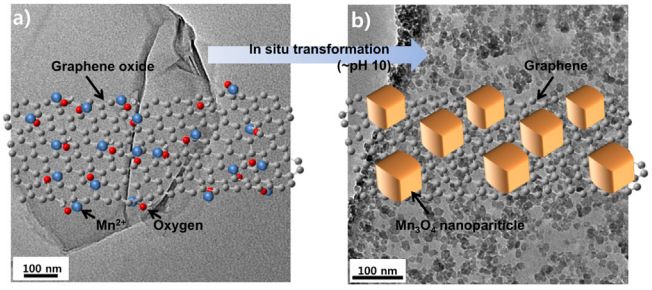

ARTICLE INFO

Article history:
Received 26 September 2012
Received in revised form
8 April 2013
Accepted 11 April 2013
Available online 20 April 2013

Keywords:
Energy storage
Graphenes
Composite materials
Lithium-ion batteries
Manganese oxides

ABSTRACT

A one step method for the fabrication of Mn_3O_4 nanoparticles/graphene composite materials is described. An in-situ transformation technique using an aqueous phase at ambient conditions is employed. During the process of forming Mn_3O_4 nanoparticles, graphene oxide is simultaneously reduced to a graphene nanosheet which simplifies the overall process and eliminates the need for an additional reduction step, which is generally energy consuming and produces toxic by-products. The resulting materials were characterized using XPS, XRD, TEM, STEM–EDS and electrochemical analysis. The Mn_3O_4 nanoparticles with uniform size (about 14 nm) and shape are highly dispersed on the surface of graphene. The material exhibits a reversible capacity of over 500 mAh g^{-1}, at a current density of 60 mA g^{-1} with less significant fades after 40 cycles. Furthermore, its rate capability and cycling stability are enhanced in comparison with that of the pure Mn_3O_4 nanoparticles.

1. Introduction

Nanostructured transition metal oxides such as FeO, CoO, Fe_3O_4 and Co_3O_4, have been extensively studied for use as an anode material for lithium-ion batteries, because of their higher specific capacities [1–5]. Mn_3O_4 is one of the most interesting materials for use as an anode for lithium-ion batteries, due to the ready availability of Mn, the fact that it is low cost, environmentally benign and has a high theoretical specific capacity (calculated to be 936 mAh g^{-1}). However, the lower electrical conductivity ($\sim 10^{-7}$–10^{-8} S cm^{-1}) of Mn_3O_4 compared with Fe_3O_4 and Co_3O_4 is a limiting factor for its use as an anode material in lithium-ion batteries. To address this, a variety of techniques have been applied in attempts to solve this problem, including the use of carbon based nanocomposites, and unique Mn_3O_4 nanostructures [6–9].

Graphene, a recently discovered allotrope of carbon, has desirable characteristics as a substrate for hosting active materials in Li

* Corresponding author. Tel.: +82 2 880 7438; fax: +82 2 888 0708.
E-mail address: jyi@snu.ac.kr (J. Yi).
[1] These authors contributed equally.

0378-7753/$ – see front matter © 2013 Elsevier B.V. All rights reserved.
http://dx.doi.org/10.1016/j.jpowsour.2013.04.055

ion batteries including a high surface area, regular frameworks, high conductivity, and chemical stability. Because of these characteristics, graphene can be used in a composite with oxide nanoparticles to improve the electrochemical performance of these particles because the graphene layers can provide a support for anchoring well-dispersed nanoparticles and can function as a pathway for the flow of electrons from the current collector to active materials [10–13].

A Mn_3O_4/graphene composite material was recently synthesized and reported to have a good rate capability, cycling stability, and a high specific capacity near the theoretical value in Li ion batteries [14]. Previous reports have appeared dealing with the fabrication of Mn_3O_4/graphene composite materials. One is a sequential method in which Mn_3O_4 nanoparticles are prepared and, then imbedded in the graphene, while other methods involve two-steps that include hydrothermal or microwave reactions of Mn precursors and a graphene oxide (GO) composite [14–16]. However, these methods are somewhat complicated or involve the use of harsh conditions and consume large amounts of energy, which makes the production of this composite material difficult and causes energy and environmental problem in large scale.

In this study, we report on the development of a one step in-situ transformation method that uses an aqueous phase for fabricating a Mn_3O_4/graphene composite for use as an anode material in Li ion batteries. The proposed method is simple, in that two reactions simultaneously occur. The first reaction is the oxidation of Mn^{2+} to Mn_3O_4 and the second reaction is the reduction of GO to produce a graphene nanosheet (GNS). In addition, the process does not involve harsh conditions, a large energy consumption and no toxic byproducts such as NOx gas are produced, because GO is not reduced by a hydrothermal reaction and chemical reduction using a toxic reagent such as hydrazine. Moreover, GO is prepared by 'improved method' that does not involve a large exotherm and produces no toxic gas compared to GO synthesized by conventional methods [17].

The prepared composite material exhibited a high specific capacity, good cycle stability and rate capability. To the best of our knowledge, this scheme is the most economical and environmentally friendly method currently available for the synthesis of a Mn_3O_4/graphene composite having high electrochemical performance.

2. Experiment details

2.1. Sample preparation

Graphite oxide was prepared by the "improved method", following a procedure reported in the literature [17]. Graphite flacks (1.5 g, Sigma Aldrich) and $KMnO_4$ (9 g, Sigma Aldrich) were mixed together and then added 9:1 mixture of concentrated H_2SO_4/H_3PO_4 (180 ml, Sigma Aldrich, 95%/20 ml, Sigma Aldrich, 85%). The mixture was maintained under vigorous stirring at 323 K for 12 h, and then was cooled to room temperature and poured onto ice (200 ml) with H_2O_2 (1.5 ml, Sigma Aldrich, 37%). After the reaction, the mixture was centrifuged at 5000 rpm for 30 min, and the supernatant was decanted and discarded. The remaining yellow solid material was then washed with water (200 ml), HCl (200 ml, Sigma Aldrich, 35%), and ethanol (200 ml) repeatedly. The material was coagulated by adding ether (200 ml, Sigma Aldrich, 99%), which resulted in yellow cloudy solution. The solution was vacuum-dried overnight at room temperature. Finally, yellow solid powders, graphite oxide, were prepared.

An Mn_3O_4 nanoparticle and graphene nanosheet (Mn_3O_4/GNS) composite was prepared using the one step in-situ transformation in an aqueous phase. A detailed description of the preparation of Mn_3O_4/GNS composite is as follows: 0.2 g of the graphite oxide, prepared *via* the improved method, was mixed in 80 ml of deionization water at room temperature, and the solution then ultrasonicated for 1 h to exfoliate graphite oxide. $MnCl_2$ solution (1.25, 2.5 and 5 ml, 0.1 M, Sigma Aldrich) was then added to the above solution. The solution was vigorously stirred for an hour, and NaOH solution (5 ml, 0.5 M, Sigma Aldrich) was added. At this point, the color of the mixture turned to black. The solid material in the black cloudy solution was isolated as a pellet by centrifugation and the resulting solid material was then washed 5 times with deionized water by further centrifugation at 10,000 rpm for 30 min each. In this step, extraneous ions, such as Na^+ and Cl^-, and extraneous GO as colloidal state (about 90% of input GO) were removed. Finally, The sample was dried for 24 h under an atmosphere at 60 °C.

2.2. Characterization of Mn_3O_4/GNS composite

The surface chemical environment, composition and shape of the samples were investigated by X-ray photoelectron spectroscopy (XPS), X-ray diffraction (XRD), transmission electron microscopy (TEM) and Scanning Transmission Electron Microscopy (STEM) analysis. XPS spectra were analyzed with a Kratos AXIS-HSi electron spectrometer equipped with a Mg-Ka X-ray source and a hemispherical electron energy analyzer. High-angle XRD, employing a Rigaku D-MAX2500-PC powder X-ray diffractometer operating at 50 kV and 100 mA with Cu Ka radiation (1.5406 Å). HR-TEM and STEM is carried out on JEOL JEM 3010 operating at 300 kV and JEOL JEM 2100F, 200 kV.

2.3. Electrochemical analysis

Electrochemical measurements were carried out using CR2032 type coin cells at room temperature. The working electrode was prepared by mixing 80 wt% of Mn_3O_4/GNS composite as the active material, 10 wt% Super P as a conductive additive, and 10 wt% poly(vinylidene difluoride) (PVDF) as a binder of the total electrode mass. The three components were mixed with *N*-methyl-2-pyrrolidone (NMP) as the solvent to produce slurry. It was uniformly loaded on a Cu foil with a doctor blade as a current collector and compressed to prepare a film-type electrode. The sample was cut into circular electrodes and dried for 12 h under vacuum at 120 °C. The cells were assembled in an Ar-filled glovebox with lithium foil as the anode, and a solution of 1.0 M $LiPF_6$ dissolved in 1:1 (v/v) EC/DEC as the electrolyte. Galvanostatic Li^+ charge/discharge analysis was carried out on wonatech WBCS3000 automatic battery cycler. All electrochemical measurements were carried out in the potential range from 0.01 V to 3 V (vs Li^+/Li).

3. Results and discussion

In this facile method, Mn_3O_4 nanoparticles are grown on GO by an in-situ transformation in an aqueous phase to produce a Mn_3O_4/GNS composite material under ambient conditions (Fig. 1). For this process, a manganese chloride precursor was dissolved in an aqueous suspension of GO. Firstly, a graphite oxide was prepared by the so-called "improved method" [17]. It has been reported that graphite oxide synthesized by this method has fewer defects in the basal plane and contains higher amounts of oxygen-containing functional groups on the surface without involving a large exotherm and producing no toxic gas, compared to graphite oxide synthesized by Hummers' method. The GO used in this reaction was prepared by exfoliation of the graphite oxide after ultrasonication treatment.

The oxygen functional groups in exfoliated GO offer the abundance of binding sites for the attachment of Mn^{2+} ions *via*

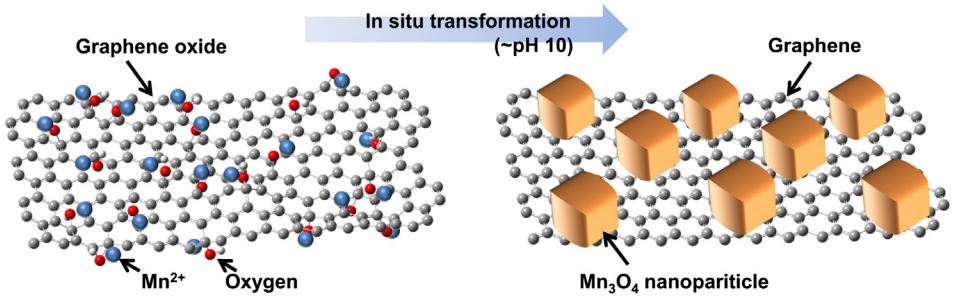

Fig. 1. The scheme for the one step in-situ transformation method that uses an aqueous phase for the fabrication of Mn_3O_4/GNS composite. Mn_3O_4 nanoparticles and GO are simultaneously reduced to GNS.

electrostatic interactions [12]. These Mn^{2+} ions are oxidized with oxygen contained in a functional group on the GO and are hydrolyzed when a NaOH solution is added. The resulting manganese hydroxide can be easily transformed to Mn_3O_4 nanoparticles under ambient conditions [18]. During this process of forming Mn_3O_4 nanoparticles, GO is simultaneously reduced to GNS which make the process simple without the need for an additional reduction step, which is generally energy consuming or produces toxic by-products. After this synthetic process, it is possible to, not only obtain the Mn_3O_4/GNS composite, but also easily control the amount of Mn_3O_4 nanoparticles on the GNS.

3.1. Characterization of Mn_3O_4/GNS composite

The chemical states of carbon species were examined by XPS analysis before and after the in-situ transformation reaction, to confirm the successful formation of a Mn_3O_4/GNS composite (Fig. 2). The XPS spectra for the C1s region are composed of three contributions at ca. 284.6, 286.7, and 288.6 eV which correspond to carbon sp^2 bonding (C—C), epoxide/hydroxyl groups (C—O), and carbonyl/carboxyl groups (C═O), respectively [19]. Before the reaction, graphite oxide showed the dominant characteristic peak indicating C—O bonds, which attribute to the presence of oxygen-containing functional groups (Fig. 2a). The proportions of which are larger than graphite oxide synthesized by other methods according to previous research [12,17,18]. However, after the in-situ transformation reaction, the peak associated with C—C bond becomes predominant while the intensity of the peaks related to oxidized carbon are significantly decreased (Fig. 2b). This indicates that large amounts of oxygen-containing functional groups associated with the formation of Mn_3O_4 nanoparticles have been removed and GO is simultaneously reduced to GNS.

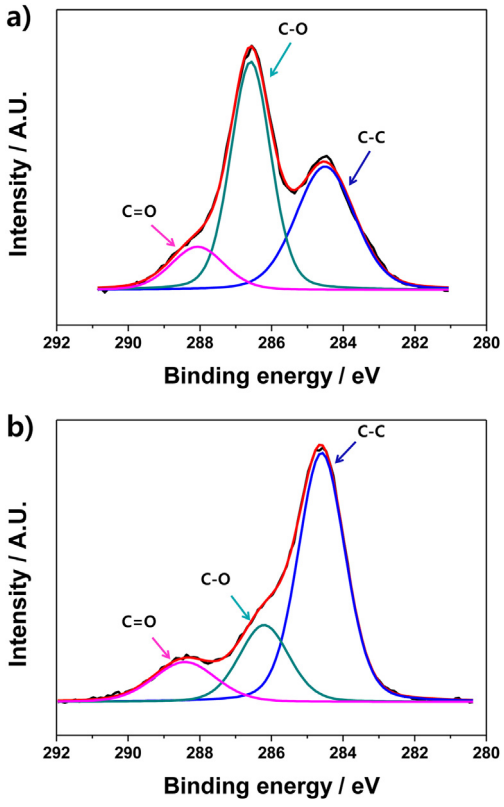

Fig. 2. XPS spectra for the C1s regions of (a) graphite oxide before the one step in-situ transformation reaction and (b) Mn_3O_4/GNS composite after the one step in-situ transformation reaction.

Compared to the XPS data for the Mn_3O_4/GNS composites, the intensity of the characteristic peaks for C═O bonds and for C—O bonds for pure GNS shows a much smaller (Fig. S1 in the Supplementary information). This verifies that the Mn_3O_4/GNS composites are still partially oxidized after the reaction. Interestingly, the intensity of the characteristic peaks for C═O bonds of Mn_3O_4/GNS composites are not changed as much as C—O bond after the reactions in the method. It is widely known that GO has its basal planes doped mainly with epoxide and hydroxyl groups, while carbonyls and carboxyl groups are located at the edges [20]. Therefore, it can be assumed that Mn_3O_4 nanoparticles are mainly formed on the surface of GNS.

The crystalline structures of both graphite oxide and Mn_3O_4/GNS composite were examined by XRD analysis in Fig. 3. The most intensive peak of graphite oxide was found at ca. 10.3° corresponding to the (001) reflection with the interlayer spacing (0.9 nm), which also indicates the introduction of rich oxygen-containing functional groups on the surface of GO (Fig. 3a). After the in-situ transformation reactions, sharp characteristic peaks were observed, indicating the formation of highly crystallized metal oxide (Fig. 3b). Their crystalline structure was found to correspond to the tetragonal structure of Mn_3O_4 (PCPDF 80-0382). The crystalline size of the synthesized Mn_3O_4 nanoparticles was found to be about 13.8 nm, as calculated by Scherrer's equation; $D = K\lambda/\beta\cos\theta$ where D is grain size of the Mn_3O_4 nanoparticles, K is the shape factor (fixed as 0.9), λ is the X-ray wavelength, β is the full width at half maximum intensity (FWHM) in radians, and θ is the Bragg angle.

The morphology of GO before the Mn_3O_4 deposition is shown in Fig. 4a. The Mn_3O_4 nanoparticles with a relatively uniform size and shape are closely attached and highly dispersed on the surface of GNS (Fig. 4a, b). The high resolution TEM images and selected area electron diffraction (SAED) patterns (inset) clearly demonstrate the presence of well textured and high crystalline shapes that are characteristic of Mn_3O_4 nanoparticles in the Mn_3O_4/GNS composite

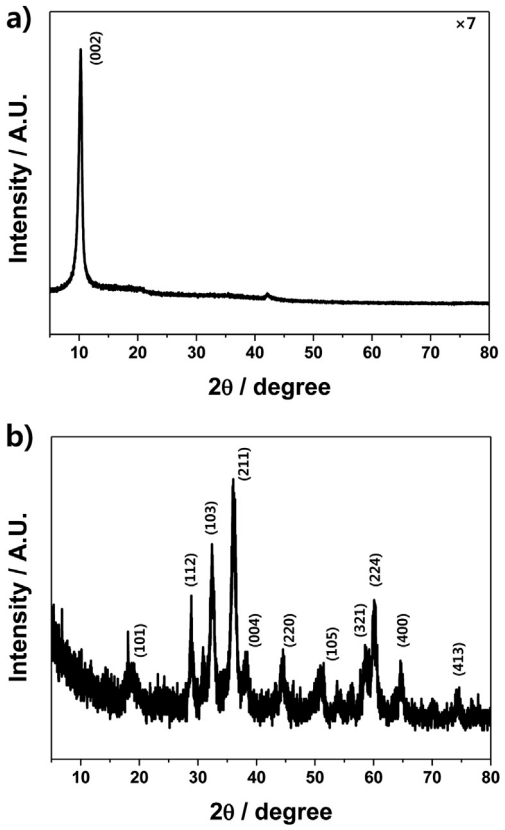

Fig. 3. XRD spectra of (a) graphite oxide before the one step in-situ transformation reaction and (b) Mn_3O_4/GNS composite after the one step in-situ transformation reaction.

(Fig. 4c). In these images, the size of Mn_3O_4 nanoparticles is approximately 14 nm, which is consistent with the crystalline size calculated from XRD spectra. The morphological properties of the Mn_3O_4/GNS composite material were also examined by HAADF–STEM analysis (Fig. 4d). The findings show that Mn_3O_4 nanoparticles are mainly located on the surface of GNS. An elemental mapping analysis for Mn and O species revealed the presence of Mn oxide nanoparticles that were well dispersion on the surface of reduced GNS (Fig. 4e, f). The anchoring of Mn_3O_4 nanoparticles to GNS enables a rapid electron transport through the underlying current collector to Mn_3O_4 nanoparticles, thus improving electrochemical performance [11,14].

3.2. Electrochemical analysis of Mn_3O_4/GNS composite

The electrochemical performance of the as-synthesized Mn_3O_4/GNS composite was evaluated in the potential range from 0.01 V to 3 V (vs Li^+/Li) using a metallic Li foil as the counter electrode (Figs. 5 and 6). The working electrode was prepared by mixing the Mn_3O_4/GNS composite, super P and poly(vinyldene fluoride) in a weight ratio of 8:1:1. A 1 M solution of $LiPF_6$ in 1:1 (v/v) ethylene carbonate (EC) and diethyl carbonate (DEC) was used as the electrolyte. Measured electrochemical characteristics are based on the mass of Mn_3O_4 as an active material. The weight of active materials used on the electrode is 0.9 mg based on Mn_3O_4 in total composite.

During the first Li ion charge (insertion) reaction, the voltage range of 1.5 to 0.4 V had an inclined curve, which results from an irreversible reaction of solid-electrolyte interface (SEI) formation (Fig. 5). In the voltage plateau around 0.4 V, Mn_3O_4 is reduced to Mn (0) and Li^+ is changed into Li_2O. The *ex-situ* XRD study of Mn_3O_4/GNS composites was conducted in order to elucidate the Li^+ insertion/extraction mechanism. In the charge reaction, Mn_3O_4 is reduced to Mn(0) and Li_2O is formed, as evidenced in Fig. S2

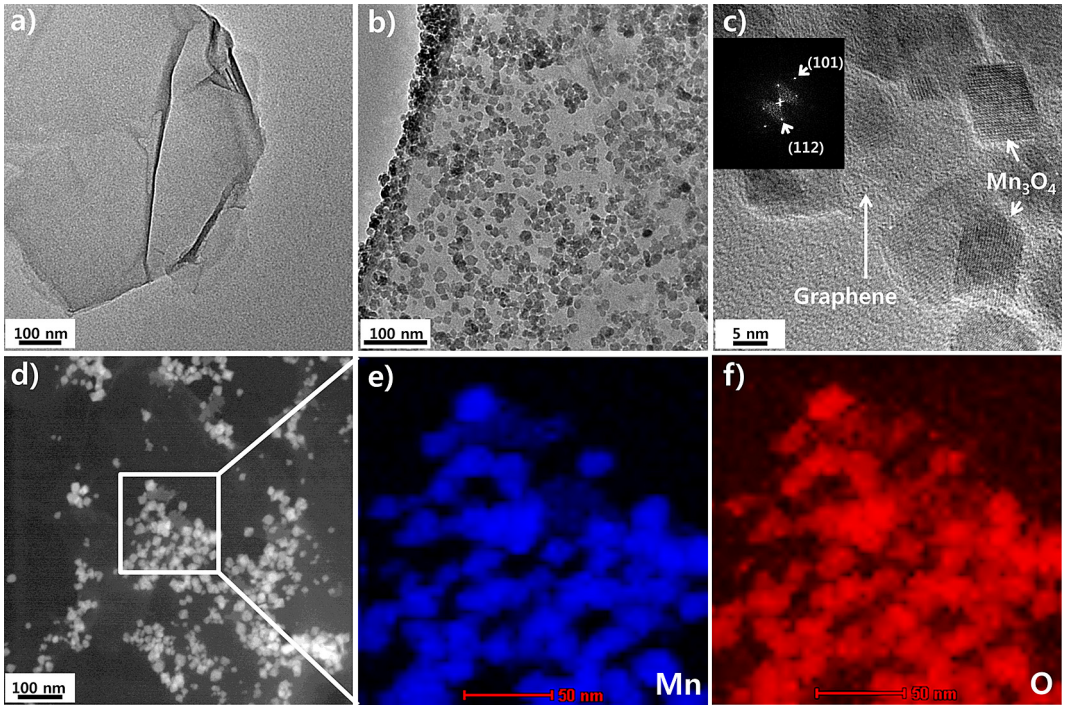

Fig. 4. TEM images of (a) GO before the one step in-situ transformation reaction, and (b) Mn_3O_4/GNS composite after the one step in-situ transformation reaction. (c) HR-TEM image of individual Mn_3O_4 nanoparticle in Mn_3O_4/GNS composite; the inset shows the electron diffraction pattern of Mn_3O_4 nanoparticle in Mn_3O_4/GNS composite. (d) HAADF–STEM image of Mn_3O_4/GNS composite and EDS element mapping results for (e) Mn and (f) O species of Mn_3O_4/GNS composite.

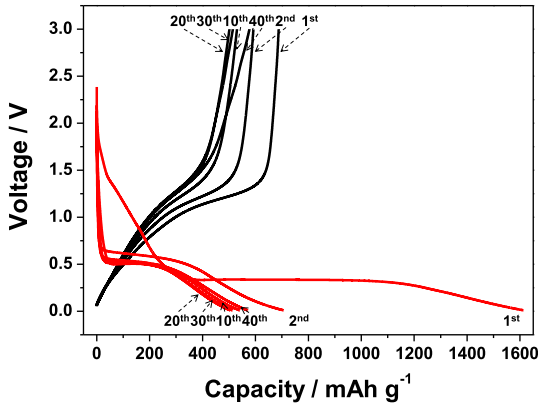

Fig. 5. Galvanostatic charge (red) and discharge (black) curves of Mn_3O_4/GNS composite at various cycles (1st, 2nd, 10th, 20th, 30th and 40th). Current density is 60 mA g^{-1}. The specific capacities are based on the mass of Mn_3O_4 in the Mn_3O_4/GNS composite. (For interpretation of the references to color in this figure legend, the reader is referred to the web version of this article.)

(Supplementary information). Interestingly, Mn oxide with amorphous structure is appeared during the reducing step [21,22]. It proves that the Mn_3O_4 lattice is collapsed and re-ordered to Mn(0) with the nanoscale domains during the Li^+ insertion step. The formation of nanoscale domains of Mn(0) and Li_2O results in the disappearance of the characteristic peaks in XRD, which is a typical phenomenon for conversion reaction [7,23]. In the discharge reaction, the XRD peaks were not reappeared because of the formation of nanoscale domains [23].

Although irreversible capacity appears from the SEI in the first cycle, highly reversible charge/discharge behavior can be observed immediately after the second cycle. The representative charge (insertion)/discharge (extraction) profiles of the Mn_3O_4/GNS composite at various current densities are shown in Fig. 6a. In Li ion insertion, the Mn_3O_4/GNS composite anode shows a plateau at around 0.6 V, which is characteristic of the Li^+ charge reaction: $Mn_3O_4 + 8Li^+ + 8e^- \rightarrow 3Mn(0) + 4Li_2O$, and the Li^+ discharge profile shows a plateau at around 1.2 V due to the reverse reaction in various current densities, which indicates that the Mn_3O_4/GNS electrode has a high rate capability and good Coulombic efficiency [9,14]. As the current density increases, reversible capacity decreases but the shape of the voltage plateaus in various current densities remain similar. It indicates that a similar phase transition reaction is occurred for Li^+ charge/discharge at a relatively high current density.

The differential capacity curve for the Li^+ second discharge at a current density of 60 mA g^{-1} shows the intense peak at around 1.2 V the same as the voltage of plateaus, which indicates a phase transition when Mn(0) is oxidized to MnO at this voltage (Fig. 6b). This value is lower than that of Co or Fe based metal oxides, including Co_3O_4, which causes the full cell with Mn_3O_4/GNS composite as an anode material and a specific cathode material to have a higher operating voltage and energy density than the other metal oxides in anode materials [1–5,11]. An additional peak at about 2.4 V is observed when Li ions are discharged, which corresponds to the further oxidation of MnO [9,14]. These results indicate that Mn_3O_4/GNS composite material exhibits a highly reversible reaction within this operating voltage range. In the differential capacity curve for charge state, only one sharp peak was observed around 0.6 V, which indicates the feature of a single phase reaction. It

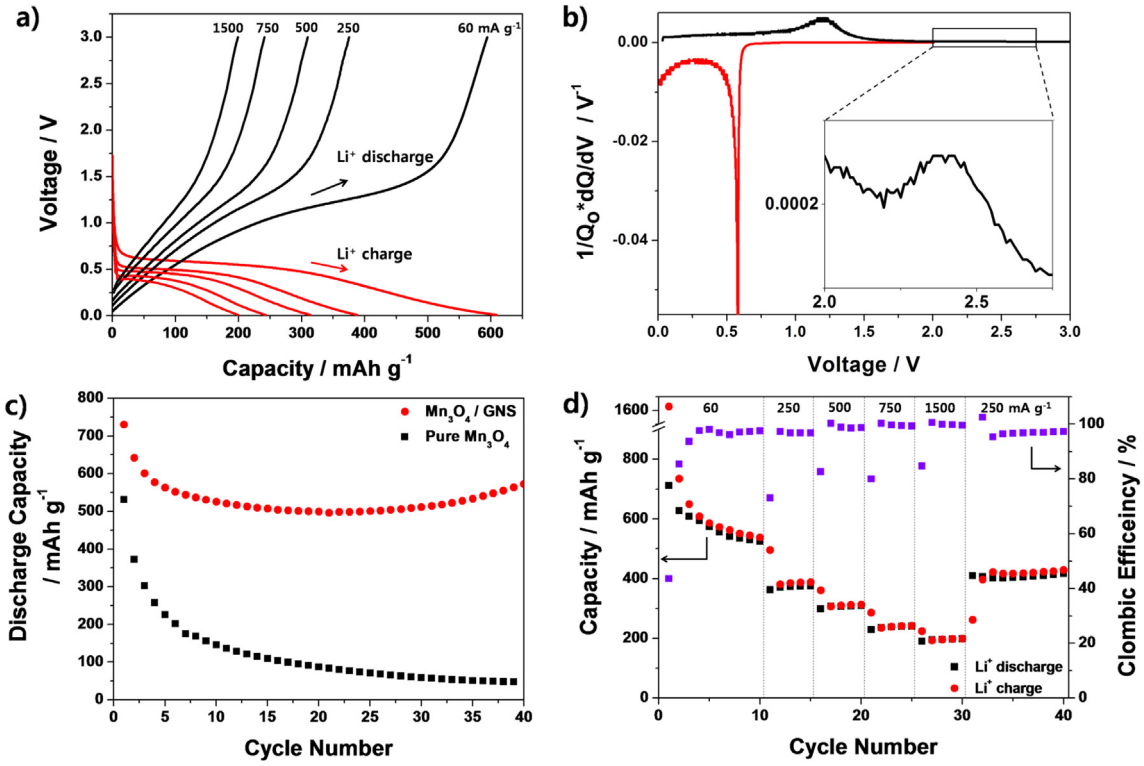

Fig. 6. (a) Representative galvanostatic charge (red) and discharge (black) curves of Mn_3O_4/GNS composite at various current densities (60, 250, 500, 750 and 1500 mA g^{-1}). (b) Differential capacity analysis of Mn_3O_4/GNS composite at second charge (red) discharge (black) step. (c) Capacity retention analysis of Mn_3O_4/GNS composite (red) and pure Mn_3O_4 nanoparticles without GNS (black) at a current density of 60 mA g^{-1}. (d) Capacity retention analysis of Mn_3O_4/GNS composite at various current densities (60, 250, 500, 750 and 1500 mA g^{-1}). The electrochemical characterizations of a half-cell composed of the Mn_3O_4/GNS composite and Li metal. The specific capacities are based on the mass of Mn_3O_4 in the Mn_3O_4/GNS composite. (For interpretation of the references to color in this figure legend, the reader is referred to the web version of this article.)

means that the lithiation reaction is very easy and the Mn_3O_4/GNS composite can maintain a good cycling performance [9].

Similar characteristic peaks -are observed in the differential capacity curve for pure Mn_3O_4 (Fig. S3a in the Supplementary information). However, the peak intensity is smaller and broadened, compared to those for the Mn_3O_4/GNS composites, indicating that the pure Mn_3O_4 has a relatively higher resistance than Mn_3O_4/GNS composites. In the control experiment, a differential capacity curve for pure GNS was examined (Fig. S3b in the Supplementary information). The GNS was fabricated by a conventional chemical reduction method using hydrazine [20]. The curve for the pure GNS does not show any characteristic peaks, which indicates that the pure GNS involves a different type of Li^+ insertion mechanism. It is well known that the two types of mechanisms for Li^+ insertion for GNS are; the formation of LiC_6 and the filling of nano-cavities between GNS by the clusters of lithium due to the scrolling and crumpling of the GNS [24–26].

The capacity for the Li^+ second discharge is 645 mAh g^{-1} and the stable discharge capacity is over 500 mAh g^{-1} at a current density of 60 mA g^{-1} exhibiting less significant fades after 40 cycles, while pure Mn_3O_4 nanoparticles showed a low Coulombic efficiency of less than 90% and a capacity lower than ~150 mAh g^{-1} after 10 cycles (Fig. 6c). Compared to pure Mn_3O_4 nanoparticles, the cycle stability of the Mn_3O_4/GNS composite electrode is significantly enhanced, which is indicative of the effect of GNS additives. As mentioned above, the main reason for the poor electrochemical characteristics of pure Mn_3O_4 electrodes is their extremely low electrical conductivity, which leads to a low reversibility and electrical disconnection between Mn_3O_4 nanoparticles and the current collector [14]. In the case of the Mn_3O_4/GNS composite, Mn_3O_4 nanoparticles are homogeneously anchored to the GNS, which results in good electrical connections between the Mn_3O_4 nanoparticle and the current collector, which would enhance electron transfer properties. Furthermore, the Mn_3O_4 nanoparticles on the surface of GNS can act as spacers to efficiently prevent the restacking of GNS. Therefore, the electrochemical performance of the Mn_3O_4/GNS composite electrode is substantially improved compared to pure Mn_3O_4.

Fig. 6d shows the capacity retention of the Mn_3O_4/GNS composite at various current densities. At 250 mA g^{-1}, the reversible capacity reaches about 390 mAh g^{-1}. Even with the increased current density of 1500 mA g^{-1}, the Mn_3O_4/GNS composite electrode can deliver a capacity close to 200 mAh g^{-1} and the capacity is maintained or even increased slightly. When the current density is 250 mA g^{-1} again, the capacity is 430 mAh g^{-1}, which shows that the Mn_3O_4/GNS electrode recovers its original capacity or becomes even slightly higher. After several Li^+ charge/discharge cycles in various current densities, the Coulombic efficiency reaches more than 99%, indicating good reversibility of the conversion reaction between Mn_3O_4 and Mn(0).

In a control experiment, the representative charge/discharge profiles for the GNS and pure Mn_3O_4 are shown in Fig. S4 (Supplementary information). The GNS shows a capacity about 300 mAh g^{-1} The portion of the Li^+ intercalation capacity of GNS in total mass of the Mn_3O_4/GNS is about 80 mAh g^{-1} because the Mn_3O_4/GNS contains about 30 wt% GNS. As the discharge capacity of the Mn_3O_4/GNS composite is about 380 mAh g^{-1} based on the total mass, GNS theoretically comprises 20% in Li^+ insertion capacity.

3.3. Adjustment of amount of Mn_3O_4 loading in composite

The amount of Mn_3O_4 nanoparticles assembled on the GNS can be adjusted without difficulty by changing the weight of $MnCl_2$ added to the reactant solution. When the weight of the $MnCl_2$ increases, the amount of the Mn^{2+} oxidized with oxygen-containing functional groups on the GNS and $Mn(OH)_2$ by the hydrolysis of $MnCl_2$ and NaOH increases, because of the supply of a larger Mn^{2+} source. When the 2.5 ml 1.0 M $MnCl_2$ solution is used, Mn_3O_4/GNS composite was produced with a loading of 72 wt% Mn_3O_4, as determined by thermogravimetric analysis (TGA). As much as half the weight of the $MnCl_2$ (1.25 ml) is transformed into a Mn_3O_4/GNS composite with a loading of 52 wt% Mn_3O_4 and when as much as 2.5 times the weight of $MnCl_2$ is used (5 ml), a composite with a loading of 81 wt% Mn_3O_4 is produced. The amount of $MnCl_2$ in the various starting solutions was 15.73, 31.46 and 62.92 mg, respectively. The amount of Mn_3O_4 in the final composite was 9.24, 18.57 and 37.01 mg, respectively. Therefore, the mass of $MnCl_2$ in the starting solution and the mass of Mn_3O_4 in the final composite product show a linear dependence. From the stoichiometric calculation, the theoretical mass of Mn_3O_4 in the final composite is 9.55, 19.08 and 38.16 mg, respectively, which are quite similar to the actual amount of Mn_3O_4 in the final composites. This verifies that Mn^{2+} ions can be fully oxidized when this method is used (Fig. S5 in the Supplementary information). XRD, TGA, and TEM images of Mn_3O_4/GNS composites with different loading weights of Mn_3O_4 are shown in Fig. S6.

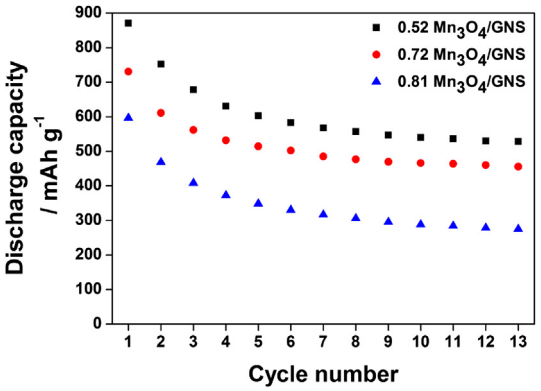

Fig. 7. Capacity retention analysis of various amount of Mn_3O_4 loading in Mn_3O_4/GNS (the weight ratio of Mn_3O_4 to total composites are 0.52, 0.72, 0.81, respectively).

The three anode materials (the composite with 52, 72 and 81 wt % Mn_3O_4) show capacities of about 600, 500 and 300 mAh g^{-1} based on the mass of Mn_3O_4, respectively. As the weight ratio of Mn_3O_4 to total composite is decreased, the capacity of the Mn_3O_4/GNS composite based on the weight of Mn_3O_4 is increased, because the electrical conductivity increased with the increase in the amount of GNS (Fig. 7). Results showed that the capacities of the Mn_3O_4/GNS composites based on the total weight of the composite are 320, 380 and 250 mAh g^{-1}, respectively. The maximum capacity was observed for a composite with ~70% Mn_3O_4 in this study.

4. Conclusion

The findings reported herein describe the use of a one step in-situ transformation in aqueous phase for the synthesis of a Mn_3O_4/GNS composite which can function as an anode material for Li ion batteries. The method is environmental-friendly and consumes minimal energy and time, in that two reactions, the first being the oxidation of Mn^{2+} to Mn_3O_4 and the second being the reduction of GO to GNS, are carried out simultaneously. The as-synthesized Mn_3O_4/GNS composite is comprised of distributed Mn_3O_4 nanoparticles with sizes about 14 m on the GNS surface, which provides a relatively higher conductivity than pure Mn_3O_4 nanoparticles. The as-synthesized composite exhibits a reversible capacity of over 500 mAh g^{-1} with less significant fades after 40 cycles and its rate capability and cycling stability are enhanced in comparison with that of pure Mn_3O_4 nanoparticles. In addition, precise sequence of the conversion reactions of Li^+ insertion/extraction process of Mn_3O_4/GNS is probed

using the differential capacity analyses and the *ex-situ* XRD analyses. This new type of in-situ transformation proposed here would provide an economical method for the synthesis of metal oxide - graphene composite materials in the area of catalysts, absorbents, super-capacitors, and Li ion batteries.

Acknowledgment

This research was supported by WCU (World Class University) program, through the National Research Foundation of Korea, funded by the Ministry of Education, Science and Technology (R31-10013).

Appendix A. Supplementary data

Supplementary data related to this article can be found at http://dx.doi.org/10.1016/j.jpowsour.2013.04.055.

References

[1] P. Poizot, S. Laruelle, S. Grugeon, L. Dupont, J.-M. Tarascon, Nature 407 (2000) 496–499.
[2] P.L. Taberna, S. Mitra, P. Poizot, P. Simon, J.-M. Tarascon, Nat. Mater. 5 (2006) 567–573.
[3] W.-M. Zhang, X.-L. Wu, J.-S. Hu, Y.-G. Guo, L.-J. Wan, Adv. Funct. Mater. 18 (2008) 3941–3946.
[4] X.W. Lou, D. Deng, J.Y. Lee, J. Feng, L.A. Archer, Adv. Mater. 20 (2008) 258–262.
[5] C. Ban, Z. Wu, D.T. Gillaspie, L. Chen, Y. Yan, J.L. Blackburn, A.C. Dillon, Adv. Mater. 22 (2010) E145–E149.
[6] Y.-G. Wang, L. Cheng, F. Li, H.-M. Xiong, Y.-Y. Xia, Chem. Mater. 19 (2007) 2095–2101.
[7] X. Fang, X. Lu, X. Guo, Y. Mao, Y.-S. Hu, J. Wang, Z. Wang, F. Wu, H. Liu, L. Chen, Electrochem. Commun. 12 (2010) 1520–1523.
[8] Y. Li, H. Tan, X.-Y. Yang, B. Goris, J. Verbeeck, S. Bals, P. Colson, R. Cloots, G.V. Tendeloo, B.-L. Su, Small 7 (2011) 475–483.
[9] J. Gao, M.A. Lowe, H.D. Abruna, Chem. Mater. 23 (2011) 3223–3227.
[10] A.K. Geim, K.S. Novoselov, Nat. Mater. 6 (2007) 183–191.
[11] S.-M. Paek, E. Yoo, I. Honma, Nano Lett. 9 (2009) 72–75.
[12] S. Chen, J. Zhu, X. Wu, Q. Han, X. Wang, ACS Nano 4 (2010) 2822–2830.
[13] K. Evanoff, A. Magasinski, J. Yang, G. Yushin, Adv. Energy Mater. 1 (2011) 495–498.
[14] H. Wang, L.-F. Cui, Y. Yang, H.S. Casalongue, J.T. Robinson, Y. Liang, Y. Cui, H. Dai, J. Am. Chem. Soc. 132 (2010) 13978–13980.
[15] B. Wang, J. Park, C. Wang, H. Ahn, G. Wang, Electrochim. Acta 55 (2010) 6812–6817.
[16] K.-H. Chang, Y.-F. Lee, C.-C. Hu, C.-I. Chang, C.-L. Liua, Y.-L. Yang, Chem. Commun. 46 (2010) 7957–7959.
[17] D.C. Marcano, D.V. Kosynkin, J.M. Berlin, A. Sinitskii, Z. Sun, A. Slesarev, L.B. Alemany, W. Lu, J.M. Tour, ACS Nano 4 (2010) 4806–4814.
[18] N.D. Kim, H.J. Yun, I.K. Song, J. Yi, Scr. Mater. 65 (2011) 448–451.
[19] V.C. Tung, M.J. Allen, Y. Yang, R.B. Kaner, Nat. Nanotechnol. 4 (2009) 25–29.
[20] S. Stankovich, D.A. Dikin, R.D. Piner, K.A. Kohlhaas, A. Kleinhammes, Y. Jia, Y. Wu, S.T. Nguyen, R.S. Ruoff, Carbon 45 (2007) 1558–1565.
[21] N.D. Kim, H.J. Yun, I. Nam, J. Yi, J. Mater. Chem. 21 (2011) 15885–15888.
[22] I. Nam, N.D. Kim, G.-P. Kim, J. Park, J. Yi, J. Nanosci. Nanotechnol. 12 (2012) 5704–5708.
[23] H. Kim, S.-W. Kim, J. Hong, Y.-U. Park, K. Kang, J. Mater. Res. 26 (2011) 2665–2671.
[24] J.R. Dahn, T. Zheng, Y. Liu, J.S. Xue, Science 270 (1995) 590–593.
[25] G. Wang, X. Shen, J. Yao, J. Park, Carbon 47 (2009) 2049–2053.
[26] R. Mukherjee, A.V. Thomas, A. Krishnamurthy, N. Koratkar, ACS Nano 6 (2012) 7867–7878.